Extracellular vesicle-mediated miR-126-3p transfer contributes to inter-cellular communication in the liver tumor microenvironment

ANURADHA MOIRANGTHEM*, PIYUSH GONDALIYA*, IRENE K. YAN, ADIL ALI SAYYED, JULIA DRISCOLL and TUSHAR PATEL

Departments of Transplantation and Cancer Biology, Mayo Clinic, Jacksonville, FL 32224, USA

Received February 5, 2022; Accepted October 24, 2022

DOI: 10.3892/ijo.2023.5479

Abstract. Extracellular vesicles (EVs) and their contents are gaining recognition as important mediators of intercellular communication through the transfer of bioactive molecules, such as non-coding RNA. The present study comprehensively assessed the microRNA (miRNA/miR) content within EVs released from HepG2 liver cancer (LC) cells and LX2 hepatic stellate cells (HSCs) and determined the contribution of EV miRNA to intercellular communication. Using both transwell and spheroid co-cultures of LC cells and HSCs, miR-126-3p within EV was established as a mediator of HSC to LC cell communication that influenced tumor cell migration and invasion, as well as the growth of multicellular LC/HSC spheroids. Manipulation of miR-126-3p either by enforced expression using pre-miR-126-3p or by inhibition using antimiR-126-3p did not alter tumor cell viability, proliferation or sensitivity to either sorafenib or regorafenib. By contrast, enforced expression of miR-126-3p decreased tumor-cell migration. Knockdown of miR-126-3p in tumor cells increased disintegrin and metalloproteinase domain-containing protein 9 (ADAM9) expression and in HSCs increased collagen-1A1 accumulation with an increase in compactness of multicellular spheroids. Within LC/HSC spheroids, ADAM9 and vascular endothelial growth factor expression was increased by silencing of miR-126-3p but diminished with the restoration of miR-126-3p. These studies implicate miR-126-3p in functional effects on migration, invasion and spheroid growth of tumor cells in the presence of HSCs, and thereby demonstrate functional EV-RNA-based intercellular signaling between HSCs and LC cells that is directly relevant to tumor-cell behavior.

Correspondence to: Dr Tushar Patel, Departments of Transplantation and Cancer Biology, Mayo Clinic, 4500 San Pablo Road, Jacksonville, FL 32224, USA
E-mail: patel.tushar@mayo.edu

*Contributed equally

Abbreviations: ADAM9, disintegrin and metalloproteinase domain-containing protein 9; CAFs, cancer-associated fibroblasts; CC, co-culture; ECM, extracellular matrix; EVs, extracellular vesicles; HSC, hepatic stellate cells; HG, high glucose; MC, monoculture; TME, tumor microenvironment; LC, liver cancer; TPM, transcripts per million; VEGF, vascular endothelial growth factor; RT, reverse transcription

Key words: hepatic carcinoma, tumor microenvironment, extracellular RNA, miR-126-3p, 3D spheroids

Introduction

The contribution of the local microenvironment to tumor cell behavior and tumor progression is well recognized. The tumor microenvironment (TME) is comprised of diverse cells, including stromal cells such as fibroblasts, myofibroblasts, endothelial cells, pericytes, adipose cells, immune and inflammatory cells, and extracellular matrix (ECM) (1,2). Stromal components within the local microenvironment may constrain tumor growth during early stages of tumor formation or may promote tumor growth in later stages. Stromal cells such as fibroblasts and mesenchymal stem cells are critical contributors to tumor growth. Interactions between tumor and stromal cells are mediated by soluble factors with growth-promoting or -inhibitory signals, cytokines or growth factors (3-5).

Liver cancer (LC) is the most common tumor type of the liver and is a leading cause of cancer-related death worldwide (6,7). LC frequently develops in the setting of chronic liver injury accompanied by a fibrotic milieu that arises from injury or inflammation-related activation of hepatic stellate cells (HSCs) (3). After activation, HSCs may trans-differentiate into myofibroblast-like cells and may proliferate, acquire contractile properties, secrete inflammatory cytokines, increase α-smooth muscle actin (α-SMA) expression and produce ECM proteins, including collagen (3,8). An active participation of stromal cells within the TME may contribute to the initiation and maintenance of carcinogenesis (5). For instance, interaction between LC cells and activated HSCs creates a permissive pro-angiogenic microenvironment with enhanced vascular endothelial growth factor A (VEGF-A) and matrix metalloprotease 9 (MMP9) production that increases migration and growth of the cancer cells (8,9).

Understanding the mechanisms by which tumor and stromal cells interact may provide valuable information regarding the role of tumor-stromal interactions in LC growth. The release of extracellular vesicles (EVs) has been recognized as a potential mechanism for intercellular communication (10,11). EVs

are a heterogeneous group of cell-derived vesicles, including exosomes (50-150 nm in size and of endosomal origin) (12) and microvesicles (100-1,000 nm in size and directly budding from the plasma membrane) (12,13), containing diverse biomolecules such as lipids, RNA, DNA and proteins, some of which may be capable of eliciting functional biological effects following their uptake by recipient cells (10,11,13). Thus, EV-mediated transfer may contribute to cell-to-cell communication in the local environment or at distant sites (14,15). EVs may be released and taken up by tumor cells as well as by stromal cells (12). However, the contribution and role of EVs as a mediator of intercellular signaling in the TME remains to be fully elucidated.

EVs have been implicated in suppressing immune responses, supporting endothelial angiogenesis and transforming benign cells, thus helping to establish a pre-metastatic niche (14). Furthermore, the RNAs encapsulated inside the EVs are protected from RNase-A, providing a consistent source that may regulate gene expression in the recipient cells and thus altering the TME (16). Even though several EV-RNAs have been identified to be present or enriched within EVs from LC cells, or implicated in LC, e.g. microRNA (miRNA/miR)-192, miR-122 and long non-coding RNA-regulator of reprogramming their contributions to intercellular interactions within the TME remain to be elucidated (13). Thus, the aims of the present study were to evaluate the role of EVs and the functional contribution of EV RNA to intercellular communications between tumor and stromal cells in the liver TME. In addition, the present study sought to identify EV-RNAs that may serve as biomarkers of TME interactions and potential targets for liver cancer.

Materials and methods

Cells and cell culture. HepG2 human LC cells were obtained from the American Type Culture collection and cells were authenticated by short tandem repeat profiling. The human HSC line LX2 was generated by Xu *et al* (17) and kindly provided by Dr Gregory J Gores (Division of Gastroenterology and Hepatology, Mayo Clinic, Rochester, Minnesota, USA). The cell lines were maintained in DMEM (Hyclone; Cytiva) supplemented with 10% FBS (Gemini Bio Products) and 1% penicillin-streptomycin (Gemini Bio Products) for individual cell culture. For co-culture studies, HepG2 ($4x10^5$) and LX2 ($1x10^5$) were seeded on cell-culture inserts (Falcon 0.4 μm pore size cell culture insert; BD Biosciences) in EV-depleted complete media in a humidified incubator at 37˚C with 5% CO_2.

Reagents. Precursor hsa-miR-126-3p (mature miRNA sequence of miR-126-3p: 5'-UCGUACCGUGAGUAAUAA UGCG-3'; cat. no. AM17100; assay ID: PM12841), negative control miRNA precursor (cat. no. AM17110), antimiR-126-3p (cat. no. AM17000; assay ID: AM12841) and negative control antimiRNA inhibitor (cat. no. AM17010) were purchased from Ambion (Thermo Fisher Scientific, Inc.). Lipofectamine® 3000 was purchased from Thermo Fisher Scientific, Inc. Regorafenib and Sorafenib were obtained from Selleck Chemicals.

3D co-culture spheroid model. 3D co-culture spheroids were generated from combining HepG2 and LX2 cells at a 4:1 ratio and using methylcellulose (18). After reaching 70% confluency, cells were trypsinized. The concentration of cells in suspension was determined and they were diluted with complete media to a concentration of $1x10^4$ cells/μl. Six-well tissue culture plates were coated with poly-2-hydroxyethyl methacrylate (pHEMA) to prepare a non-adherent surface. 2 μl of cell suspension was injected in a 3% w/v methylcellulose (MilliporeSigma; Merck KGaA) matrix to generate spheroids with $2x10^4$ cells each. After 3 days, the spheroids were manually retrieved from the methylcellulose matrix and cultured in fresh DMEM-high glucose (HG) media for further study.

Live/dead cell imaging in 3D co-culture spheroid model. At day 3 of 3D co-culture in methylcellulose, the spheroids were retrieved in complete DMEM-HG media for live/dead cell imaging. The harvested spheroids were then stained in a 2 μM of calcein AM and 2 μM of ethidium bromide homodimer mixture for 5 min at room temperature, followed by a wash in PBS. The stained spheroids were observed under an LSM880 confocal laser scanning microscope (Carl Zeiss AG) (18).

Histological and immunohistochemical analysis. The histological analysis was performed as per a previously described protocol. In brief, harvested spheroids were fixed in 4% paraformaldehyde for 15 min at room temperature, followed by sectioning. For morphological analysis, spheroids sections were stained with hematoxylin and eosin (H&E) (18). Furthermore, α-SMA staining in spheroids was performed as per a previous protocol (19). Immunohistochemical staining was performed using anti α-SMA rabbit polyclonal antibody (cat no. Ab5694; 1:200 dilution; Abcam) and horseradish peroxidase labeled goat anti-Rabbit antibody (cat. no. AB_2630375; Dako; Agilent Technologies, Inc.) along with 3,3-diaminobenzidine (Dako; Agilent Technologies, Inc.).

miRNA transfection of 2D cells and 3D co-culture spheroids. For 2D culture, HepG2 cells were seeded in 6-well plates ($5x10^5$/well) in 2 ml complete media and transfected with 100 nM of precursor or antimiR-126-3p using Lipofectamine® 3000 in OptiMEM (Thermo Fisher Scientific, Inc.) at 70-80% confluency. After 24 h, the OptiMEM was replaced with complete media. For co-culture of HepG2+LX2 cells as 3D spheroids, 25 spheroids per group were transferred with 500 μl OptiMEM media into a 24-well plate precoated with pHEMA. Spheroids were transfected with 200 nM of miR-126-3p precursor and antimiR-126-3p or respective negative control. After 24 h, the media was replaced with 500 ml of complete media. The spheroids were collected for further experiments 48 h after transfection.

EV isolation and characterization. HepG2 EVs were isolated by sequential ultracentrifugation and the pellets were re-suspended in PBS, as described in a previous study by our group (20). The EV concentration was determined by nanoparticle tracking analysis (NTA) using a Nanosight LM10 (Nanosight Ltd.). In brief, the solution of diluted EVs was loaded into the LM10 instrument and a series of three one-minute videos were captured of different fields of view. The average particle concentration and size parameters were calculated.

RNA isolation and sequencing. Total cellular RNA was isolated using TRIzol (Thermo Fisher Scientific, Inc.). For isolation of EV-RNA, cells were cultured in monoculture or 2D co-culture. After 48 h, the media was removed and centrifuged at 3,000 x g for 15 min, EVs were isolated using ExoQuick-TC (System Biosciences, LLC) and EV-RNA was isolated using SeraMir (Systems Biosciences, LLC). The final concentration of the cellular RNA or EV-RNA was measured using a NanoDrop 2000c Spectrophotometer (Thermo Fisher Scientific, Inc.). RNA sequencing was performed by Exiqon (Qiagen Sciences, Inc.).

Generation of cDNA. Isolated RNAs were first treated with DNase. Reverse transcription (RT) was performed using a TaqMan MicroRNA RT kit (Applied Biosystems; Thermo Fisher Scientific, Inc.) using 100 ng total RNA in a reaction mixture containing 0.15 μl 100 mM dNTPs, 1 μl reverse transcriptase, 1.5 μl 10X RT buffer, 0.19 μl RNase inhibitor and 3 μl of 5X RT primer specific for miR-126-3p (cat. no. 4427975; assay ID: 002228; Ambion; Thermo Fisher Scientific, Inc.). U6snRNA (cat. no. 4427975; assay ID: 001973; Ambion; Thermo Fisher Scientific, Inc.) was used as an internal control for the normalization of miR-126-3p expression in the experimental groups. The reactions were performed using a MyCycler™ Thermal Cycler (Bio-Rad Laboratories, Inc.) for 30 min at 16˚C, 30 min at 42˚C and 5 min at 85˚C, followed by a hold at 4˚C.

Droplet digital PCR (ddPCR). Synthesized cDNA (4 μl) was used for amplification in a 22-μl reaction volume containing 10 μl 2X ddPCR Supermix (Bio-Rad Laboratories, Inc.), 1 μl of 20X TaqMan miRNA PCR primer probe set of miR-126-3p (cat. no. 4427975; assay ID: 002228; Ambion; Thermo Fisher Scientific, Inc.), U6snRNA (cat. no. 4427975; assay ID: 001973; Ambion; Thermo Fisher Scientific, Inc.) and 7 μl nuclease-free water. Of this PCR mixture, 20 μl were loaded onto the middle wells of the Droplet Generator cartridge (Bio-Rad Laboratories, Inc.) with 70 μl of droplet generation oil (Bio-Rad Laboratories, Inc.) in the lower wells. For all assays, duplicate samples and a no template control were included. Droplets were generated using a QX200 Droplet Generator (Bio-Rad Laboratories, Inc.) and then transferred to a 96-well PCR plate. PCR amplification was performed using a C1000 Touch Thermal Cycler (Bio-Rad Laboratories, Inc.) at 95˚C for 10 min, followed by 40 cycles of 94˚C for 30 sec and 60˚C for 60 sec (ramping rate reduced to 2%), and a final elongation step at 98˚C for 10 min. The plate was then loaded into the QX200 Droplet Reader (Bio-Rad Laboratories, Inc.) and the copies of miRNA were quantitated by counting the number of positive droplets with analysis performed using the QuantaSoft software™ (version 1.7.4.0917; Bio-Rad Laboratories, Inc.).

Real-time qPCR. Real-time PCR for miR-126-3p was performed using TaqMan miRNA assays (miR-126-3p: Cat. no. 4427975; assay ID: 002228; Ambion; Thermo Fisher Scientific, Inc.; and U6snRNA: Cat. no. 4427975; assay ID: 001973; Ambion; Thermo Fisher Scientific, Inc.) as per the manufacturer's protocol. PCR amplification was performed using a Light cycler 96 thermal cycler (Roche Diagnostics) at 95˚C for 10 min, followed by 40 cycles of 95˚C for 10 sec and 60˚C for 60 sec. The threshold Cq was normalized with U6snRNA used as an endogenous control. The relative amount of miR-126-3p expression was calculated using the comparative Cq method (21). Real time-qPCR for disintegrin and metalloproteinase domain-containing protein 9 (ADAM9), CRK like proto-oncogene, adaptor protein (CRKL), CRK and GAPDH expression were performed using the following primers: ADAM9 forward, 5'-AGACAGCCGGGGAGTG TTCCTC-3' and reverse, 5'-AGGTGGCCTTGATGGGAA CTGCT-3'; CRK forward, 5'-AGGGTTATCCAGAAGCGA GTC-3' and reverse, 5'-CTTCCCACTGACCACTCACAT-3', CRKL forward, 5'-GTGCTTATGACAAGACTGCCT-3' and reverse, 5'-CACTCGTTTTCATCTGGGTTT-3'; collagen-1A1 forward, 5'-CAGGTCTCGGTCATGGTACCT-3' and reverse, 5'-GTCGAGGGCCAAGACGAA-3'; GAPDH forward, 5'-GAGTCAACGGATTTGGTCGT-3' and reverse, 5'-TTG ATTTTGGAGGGATCTCG-3'; 18S forward, 5'-GTAACC CGTTGAACCCCATT-3' and reverse, 5'-CCATCCAATCG GTAGTAGCG-3' using SYBR green (22). PCR amplification was performed using the light cycler 96 with pre-incubation at 95˚C for 120 sec, amplification at 40 cycles of 95˚C for 30 sec, 60˚C for 30 sec and 72˚C for 30 sec and then a final extension at 72˚C for 5 min.

Western blot analysis. Protein lysates were prepared using RIPA buffer and the total protein concentration was determined by using a BCA protein kit (Thermo Fisher Scientific, Inc.) (23). Subsequently, 30 μg of total protein was separated on NuPAGE-Tris Mini Gels (Novex; Thermo Fisher Scientific, Inc.). The separated proteins were then transferred onto nitrocellulose membrane (Invitrogen; Thermo Fisher Scientific, Inc.) using the iBlot-2 system (Invitrogen; Thermo Fisher Scientific, Inc.). After transfer, the membrane was blocked using intercept® blocking buffer (LI-COR Biosciences) for 1 h at room temperature, followed by overnight incubation at 4˚C with the following primary antibodies: Rabbit monoclonal antibody (mAb) to ADAM9 (cat. no. 4151S; 1:1,000 dilution; Cell Signaling Technology, Inc.), goat polyclonal Ab to β-actin (cat. no. sc-1616; 1:1,000 dilution; Santa Cruz Biotechnology, Inc.), rabbit mAb to CD9 (cat. no. 13174S; 1:1,000 dilution; Cell Signaling Technology, Inc.) and mouse mAb to CD81 (cat. no. sc-166029; 1:1,000 dilution; Santa Cruz Biotechnology, Inc.). Target proteins were detected using secondary antibody 1:15,000 dilution (IRDye 680RD donkey anti-goat secondary antibody; cat. no. 926-6807, IRDye 800CW goat anti-rabbit IgG secondary antibody; cat. no. 926-32211 IRDye® 800CW goat anti-mouse IgG secondary antibody; cat. no. 926-32210, LI-COR Biosciences) for 1 h at room temperature. Visualization was performed using the Odyssey Imaging system (LI-COR Biosciences). β-actin expression was determined concomitantly and used to normalize the protein expression.

VEGF ELISA. The VEGF expression was assessed by ELISA as per the manufacturer's protocol (cat. no. ab100662; Abcam) (24). In brief, the samples were added into the wells and incubated at room temperature for 2.5 h. Subsequently, the wells were washed and incubated with biotinylated antibody, followed by incubation with horseradish peroxidase-conjugated

streptavidin. The wells were washed, incubated with substrate solution and the reaction was terminated using stop solution. Finally, the absorbance of the wells was read at 450 nm using the FLUOstar Omega multimode microplate reader (BMG Labtech).

Proliferation assay. Cell proliferation was assessed at various time-points after transfection with precursor or antimiR using the MTS assay (25). In brief, miR-126-3p precursor or antimiR-126-3p or their respective NC-transfected cells were seeded in a 96 well plate ($1x10^4$ cells/well). For assessing proliferation, cells were incubated with MTS reagent for 2-3 h and absorbance was measured at 490 nm using the FLUOstar Omega multimode microplate reader (BMG LABTECH).

Migration and invasion assay. HepG2 cells were transfected with precursor miR-126-3p and then seeded ($1x10^5$ cells/well) in the upper chambers of Transwell inserts (8-μm pore size Falcon cell culture inserts; BD Biosciences) in serum-free media, while the lower chamber was filled with complete media. For invasion studies, wells were coated with Matrigel® (Corning, Inc.). After 24 h, non-migrated cells in the upper chamber were removed using a cotton swab, migrated cells on the lower surface of the chamber were carefully washed with PBS and fixed with 4% paraformaldehyde for 10 min at room temperature. The fixed cells were then again carefully washed with PBS and stained with 0.1% crystal violet for 15 min at room temperature. Images were captured from five different fields and the total number of migrated cells was quantitated using Wimasis image analysis (https://www.wimasis.com/en/; Wimasis GmbH).

Cell viability assay. HepG2 cells were transfected with precursor or antimiR-126-3p. After 24 h, cells were treated with 350 nM Sorafenib (Selleckchem) or 1 μM Regorafenib (Selleckchem) in DMSO (final concentration of DMSO was kept at <1%) and cell viability was assessed at different time-points using the MTS assay as described above.

In-vitro tumorigenic assay. AntimiR-126-3p-transfected LX2 cells were used for this assay. In brief, HepG2 and LX2 cells were mixed at a 1:1 ratio with 3,000 cells each and seeded in ultra low-attachment plates (cat. no. 07200603; Corning; Thermo Fisher Scientific, Inc.) to generate tumor spheres. Images were captured at various time-points. The number and size of tumor spheres formed were determined by image analysis using Image Pro Plus software version 6.0 (Media Cybernetics).

Statistical analysis. All analyses were performed using GraphPad Prism 8 (GraphPad Software, Inc.). Differences between the Pre-miR-NC/AntimiR-NC and pre-miR-126/AntimiR-126 groups were analyzed by Student's t-test (two-tailed, unpaired), while one-way analysis of variance (Tukey's multiple-comparisons test) was used to compare three or more groups. All experiments were performed in triplicate with three independent replicates. $P<0.05$ was considered to indicate statistical significance. Values are expressed as the mean ± standard deviation.

Results

Cellular and EV miRNA content in HepG2 and LX2 cells. First, the levels of characteristic extracellular RNAs were determined within EVs released from LC cells (HepG2) or HSCs (LX2) in culture, either alone in monoculture or in co-culture with each other (Fig. 1A). The size distribution was analyzed using NTA (Fig. S1A), and CD9 and CD81 surface protein expression was determined by western blot to characterize the isolated vesicles (Fig. S1B). In order to identify the miRNA, RNA sequencing was performed using RNA obtained from cells or from the EV released from the cells. The miRNA expression profiles in cells and EVs released from these cells in monoculture and co-culture settings were depicted in heatmaps in Fig. S1C.

A total of 261 distinct cellular miRNAs and 233 EV miRNAs were detected from HepG2 cells, whereas 311 cellular miRNAs and 264 EV miRNAs were identified from LX2 cells in monoculture. Of these, 176 miRNAs were found in both cells and EVs from either HepG2 or LX2 cells (Fig. 1B). In co-culture settings, 250 cellular and 196 EV miRNAs were identified from HepG2 cells during co-culture with LX2 cells. Similarly, 311 cellular and 276 EV miRNAs were identified from LX2 cells co-cultured with HepG2 cells. 154 miRNAs were detected in both the cells and EVs of either HepG2 or LX2 (Fig. 1B).

MiRNAs that were expressed in HepG2 cells in monoculture and in co-culture with LX2 cells were then identified (Fig. 1C-F). A total of 246 miRNAs were common to both cell types (Fig. 1G). Amongst these, 22 miRNAs were increased by >2 fold in HepG2 during co-culture of these cells with LX2 cells (Table SI). Among the top 5 miRNAs that were increased in HepG2 cells, miR-126-3p was also highly expressed in LX2, cells as well as in the EVs released from LX2 cells (Table SII). Therefore, the expression of miR-126-3p was further validated by PCR with quantitative analysis by ddPCR, revealing 116 copies/μl of miR-126-3p in HepG2 cells co-cultured with LX2 compared with 14 copies/μl in HepG2 cells in monoculture (Fig. 1H). These results indicated that co-culture of HepG2 cells resulted in an increase in miR-126-3p in HepG2 cells, and that this may involve the transfer of miR-126-3p in EV from LX-2 cells.

Alteration of tumor cell phenotype by miR-126-3p. To determine the cellular effects of alterations in cellular miR-126-3p expression that occur during co-culture, the effect of modulation of miR-126-3p expression on cell viability was assessed. HepG2 cells were transiently transfected with either pre-miR-126-3p to enhance expression or antimiR-126-3p to reduce expression (Fig. S1D and E). Target gene expression studies verified the effects of transfection of these constructs compared with their respective controls. Cell proliferation was assessed over a 72-h period in cells following transient transfection with pre-miR-126-3p or antimiR-126-3p, but no difference was observed with either construct (Fig. 2A and B). The effect of modulation of miR-126-3p on the cellular response to therapeutic drugs was then further evaluated. HepG2 cells were transfected with either pre-126-3p or antimiR-126-3p or their respective controls prior to exposure for 72 h to either sorafenib or regorafenib. However, modulation of miR-126-3p did not

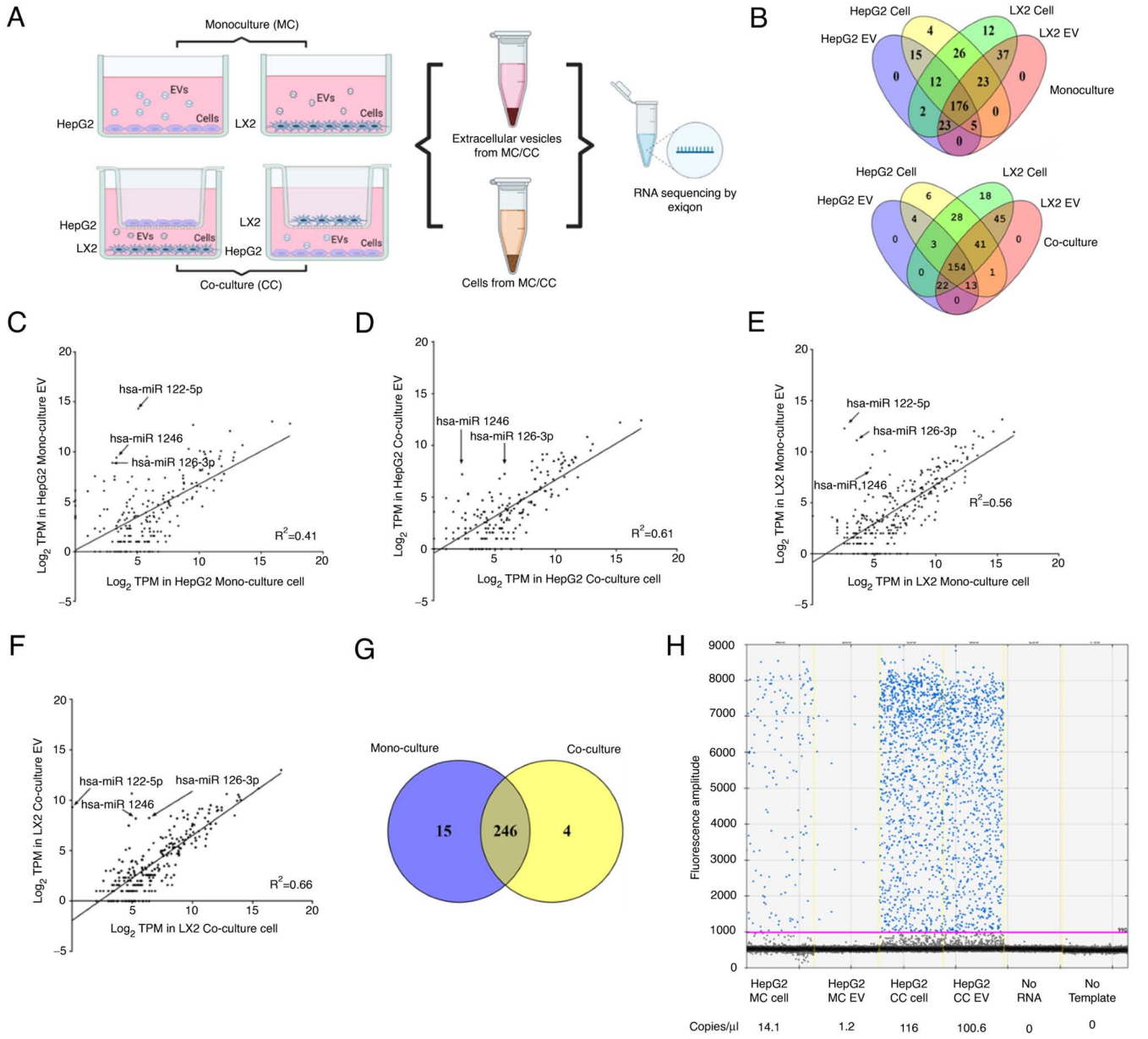

Figure 1. Cellular and EV RNA in cells and EV released from cells. (A) Experimental set-up design for the *in vitro* co-culture between HepG2 and LX2 cells. HepG2 cells and LX2 cells were cultured alone or together as indirect co-culture using cell culture inserts. RNA was isolated from the cells and EVs released by monoculture and co-cultured cells. Small RNA sequencing and analysis of miRNA expression was performed. (B) The number of miRNAs identified in each is illustrated. (C and D) Plots of miRNA gene expression in cells vs. miRNA expression in EV released from these cells for HepG2 cells in (C) monoculture and (D) co-culture, and (E and F) for LX-2 cells in (E) monoculture and (F) co-culture. Values are expressed as log2TPM. (G) HepG2 or LX2 cells were maintained in co-cultures with each other in Transwells, as illustrated. RNA was isolated from cells in the bottom chambers of the Transwell or EVs released from these cells. The numbers of miRNAs identified in HepG2 cells and EV and LX2 co-cultured cells and EV are presented in a Venn diagram. (H) Validation of miR-126-3p by digital PCR. RNA was isolated from HepG2 cells or EVs released from these cells when maintained in monoculture or in co-culture with LX2 cells. Expression of miR-126-3p was assessed using droplet digital PCR. Taqman Assay PCR samples were partitioned using the Droplet Generator and thermal cycled to the end-point. A droplet reader was used to read each droplet and results were analyzed using QuantaSoft version 1.7.4.0917 (all from Bio-Rad Laboratories, Inc.). Fig. 1A was generated using BioRender.com. EV, extracellular vesicle; TPM, TPM, transcripts per million; miRNA/miR, microRNA; CC, co-culture; MC, monoculture.

alter the sensitivity of HepG2 cells to either drug (Fig. 2C-F). Next, the effects of modulation of miR-126-3p on migration and invasion, malignant cellular phenotypes associated with tumor behavior, were examined. Enforced expression of miR-126-3p by transient transfection with precursor miR-126-3p decreased cell migration compared to that of cells transfected with NC precursor (Fig. 3A and B). Similarly, a decrease in HepG2 cell invasion across Matrigel was observed with miR-126-3p over-expression (Fig. 3A and C). To further evaluate the phenotypic effects of altered miR-126-3p on tumorigenesis, miR-126-3p was downregulated in LX2 cells using antimiR-126-3p (Fig. 4A) and HepG2/LX2 cell spheroids were generated using these cells. Of note, these spheres were more compact (Fig. 4B) but similar in size (pixel size in diameter) compared with HepG2/LX2 spheroids formed using LX2 cells transfected with negative inhibitor of miR-126-3p (Fig. 4C). However, there was no considerable change in the number of spheroids formed between the two groups (Fig. 4D). Consistent with this, an

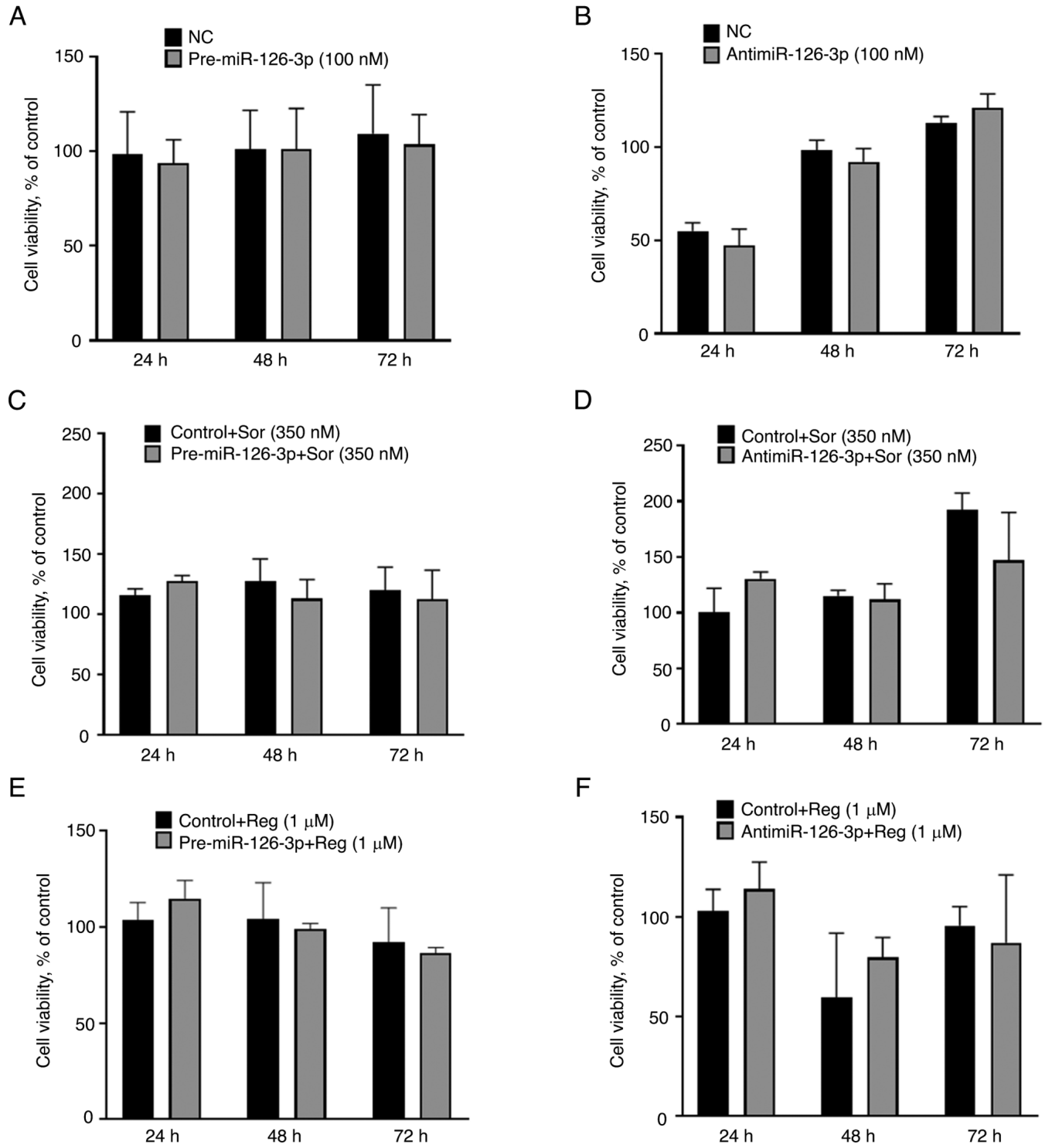

Figure 2. Effect of miR-126-3p on cell proliferation and chemosensitivity. (A and B) Cell proliferation assay was performed after transfecting HepG2 cells with either (A) miR-126-3p precursor or negative precursor, or (B) antimiR-126-3p or negative inhibitor. (C and D) HepG2 cells were transfected with (C) precursor to miR-126-3p or control precursor, or (D) antimiR-126-3p or a non-targeting control antimiR and incubated with 350 nM sorafenib after 24 h. (E and F) HepG2 cells were transfected with (E) precursor to miR-126-3p or control precursor, or (F) antimiR-126-3p or a non-targeting control antimiR and incubated with 1 μM regorafenib after 24 h. At the indicated time-points, cell viability was assessed using the MTS assay. Values are expressed as the mean ± standard deviation (n=3 replicates). miR, microRNA; NC, negative control; Sor, sorafenib; Reg, regorafenib.

increase in collagen-1A1 was observed following knockdown of miR-126-3p in LX2, indicating ECM production (Fig. 4E).

Downstream targets of miR-126-3p in cancer cells. In order to identify potential intercellular targets of miR-126-3p that may contribute to phenotypic changes, including cell migration, a TargetScan search (https://www.targetscan.org/vert_80/) was performed, which identified 28 predicted targets. Amongst these, ADAM9, CRK and CRKL have been reported to be involved in inducing cancer cell migration (26-28). Therefore, the effects of antisense-mediated inhibition of miR-126-3p on the expression of these genes were experimentally determined.

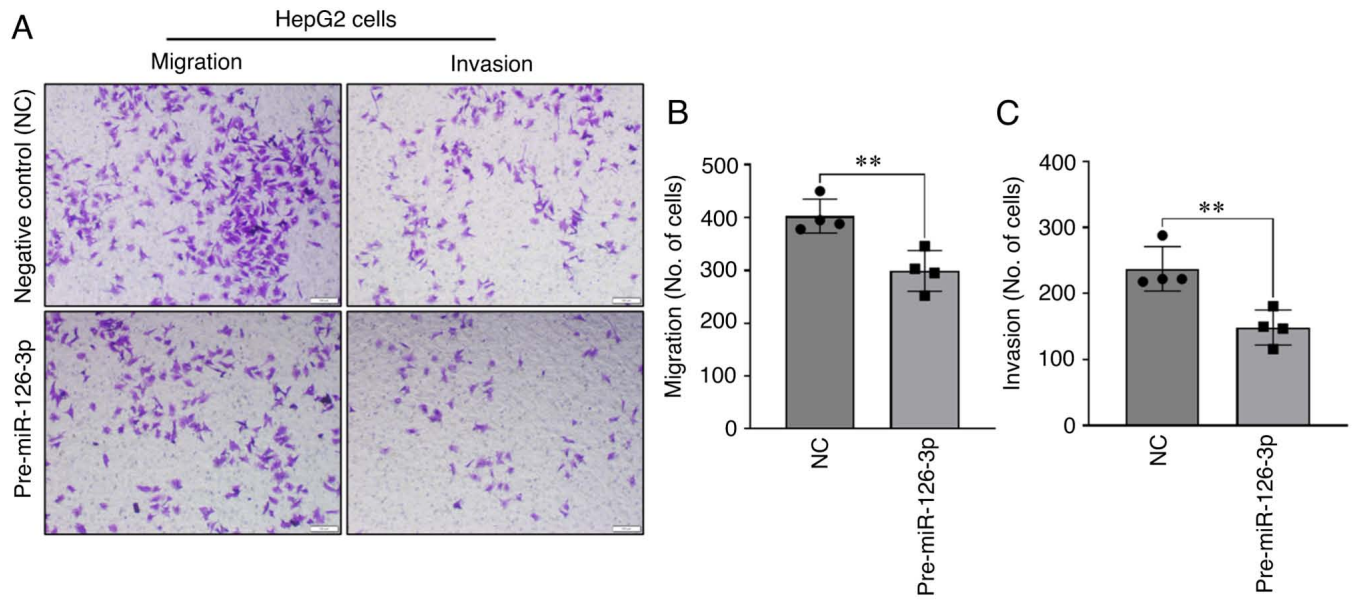

Figure 3. Effect of miR-126-3p on cell migration and invasion. HepG2 cells were transfected with precursor to miR-126-3p or control precursor. (A) Representative images of cell migration and invasion across the Transwell membrane after staining with crystal violet (scale bars, 100 μm). Quantitation of number of cells with (B) migration or (C) invasion across the Transwell membrane. Values are expressed as the mean ± standard deviation (n=3 replicates). **P<0.01. miR, microRNA; NC, negative control.

Transient transfection with antimiR-126-3p significantly decreased miR-126-3p expression in HepG2 cells (Fig. S1E). Concomitantly, the expression of ADAM9 mRNA, but not CRK and CRKL, was increased in cells transfected with antimiR-126-3p compared to negative control transfectants (Fig. 4F). These findings suggest that miR-126 downregulation is linked to ADAM9 expression in LC to regulate cancer metastasis, invasion and chemoresistance.

Modulation of tumor and stromal cell spheroid growth by miR-126-3p. Cells in 2D cultures may not fully recapitulate *in vivo* situations due to lack of cell-cell interaction. To further assess the effect of tumor-stromal interactions *in vitro*, a multicellular spheroid model comprised of LC cells and HSCs was generated. A previously reported methyl cellulose-based 3D co-culture model was used (Fig. 5A) (18). Spheroids were first generated using a 1:1, 4:1 and 24:1 ratio of HepG2 to LX2 cells (Fig. S2). After 3 days, the 4:1 ratio resulted in a more compact spheroid, which is more physiologically relevant (Fig. 5B). Confocal microscopy after live/dead staining revealed non-viable cells in a central necrotic core (Fig. 5C). The cell distribution in the spheroid was assessed by H&E staining (Fig. 5D). Activation of HSC is known to increase the expression of α-SMA within the LC TME (29), which was confirmed in the present study by immunohistochemical staining of 3D-co-culture spheroids (Fig. 5D). These results corroborated the previous findings that, compared with cell spheroids generated from LC cells alone, multicellular spheroids generated from co-cultures of LC cells and HSCs were more compact than spheroids comprised of LC cells alone (9). Next, the expression of miR-126 in 3D HepG2/LX2 spheroids was determined using real-time qPCR. Of note, miR-126 was downregulated in the multicellular spheroids compared with spheroids generated only from HepG2 cells in contrast to the results from 2D culture (Fig. 5E).

Modulation of expression of downstream targets in LC/HSC spheroids by miR-126. In the current 2D culture settings, miR-126-3p modulation resulted in regulation of ADAM9 in HepG2 cells. Hence, the expression level of the downstream candidate target of miR-126-3p, ADAM9, was evaluated in 3D spheroids. In multicellular spheroids, the mRNA level of ADAM9 was increased compared with that observed in HepG2-only unicellular spheroids (Fig. 5F). Increased ADAM9 protein expression was likewise confirmed by western blot analysis (Fig. 5G and H). Previously, miR-126-3p has also been reported to target VEGFA to modulate angiogenesis (30). Therefore, the present study investigated the expression of VEGFA protein in the co-culture system. ELISA confirmed that VEGFA protein was upregulated in multicellular spheroids compared to monocellular ones (Fig. 5I). Next, to determine the effect of alterations in expression of miR-126-3p on ADAM9 and VEGFA, HepG2/LX2 spheroids were transfected with either pre-miR-126-3p or antimiR-126-3p. Overexpression and knockdown of miR-126 was confirmed by real time-qPCR (Fig. 6A and B, respectively). The target gene effects were verified by real time-qPCR: ADAM9 mRNA and protein were reduced, and VEGF expression was also reduced after transfection with pre-miR-126. On the other hand, antimiR-126 increased ADAM9 expression as well as VEGFA protein expression (Fig. 6C-H). These results validated the findings from the *in vitro* 2D experiments.

Discussion

Tumor cells frequently arise in the setting of a fibrotic milieu or may be accompanied by HSCs. The presence of activated HSCs contributes to hepatic fibrosis and comprises an essential element of the tumor stroma (31). Activation of focal adhesion kinase-MMP9 signaling by HSC in the TME promotes LC cell migration and invasion (32) and the presence of HSCs in

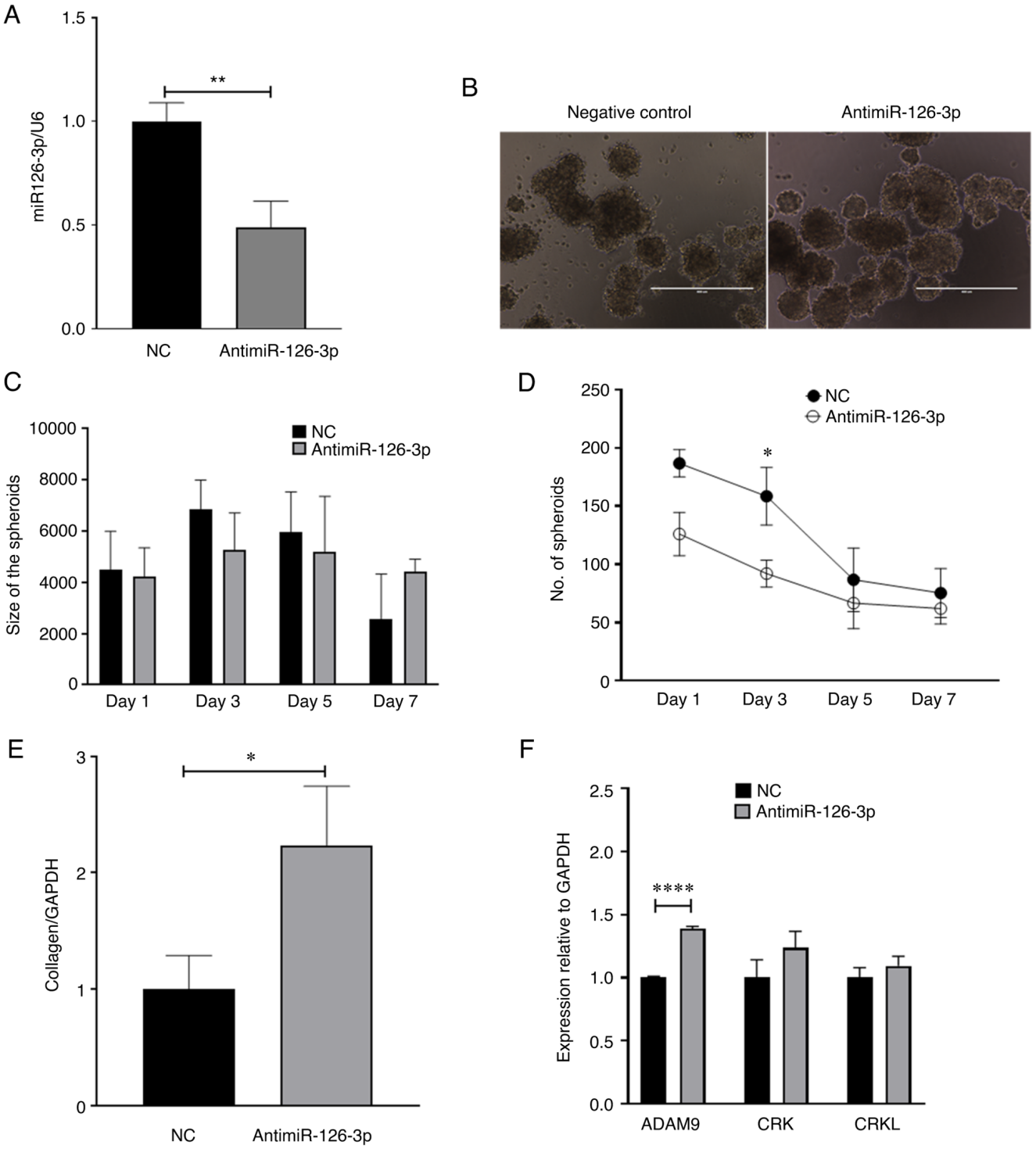

Figure 4. Effect of miR-126-3p knockdown in LX2 cells and HepG2 cells. LX2 cells were transfected with antimiR-126-3p or a non-targeting control antimiR for 48 h. Transfected LX2 cells were then cultured with HepG2 cells in low-attachment conditions and spheroid growth was assessed. (A) Real time-qPCR analysis of miR-126-3p expression in LX2 cells transfected with antimiR-126-3p. Data represent the fold change relative to the control after normalization to U6snRNA as an internal control. (B) Microscopy of spheroids indicated increased compactness in the antimiR-126-3p group compared with the negative control (scale bars, 400 μm). (C) Spheroid size (pixel size in diameter) and (D) number of spheroids were determined at the indicated times after cultures were initiated. (E) Real time-qPCR analysis of collagen-1A1 expression in LX2 cells transfected with antimiR-126-3p. Data represent the fold-change relative to control after normalization to GAPDH as an internal control. (F) Real time-qPCR analysis of ADAM9, CRK and CRKL expression. Data represent the fold change relative to control after normalization to GAPDH as an internal control. Values are expressed as the mean ± standard deviation (n=3 replicates). *P<0.05, **P<0.01, ****P<0.0001. ADAM9, disintegrin and metalloproteinase domain-containing protein 9; CRKL, CRK like proto-oncogene, adaptor protein; miR, microRNA; NC, negative control; qPCR, quantitative PCR.

the microenvironment contributes to LC chemoresistance by secretion of hepatocyte growth factor (33). Secretion of laminin 5 in the tumor milieu by activated HSCs may stimulate the migratory ability of LC (34). In a co-culture study of LC and HSC, CD147 was identified as a key molecule in inflammation and cancer (35). Furthermore, glypican 3 has been identified

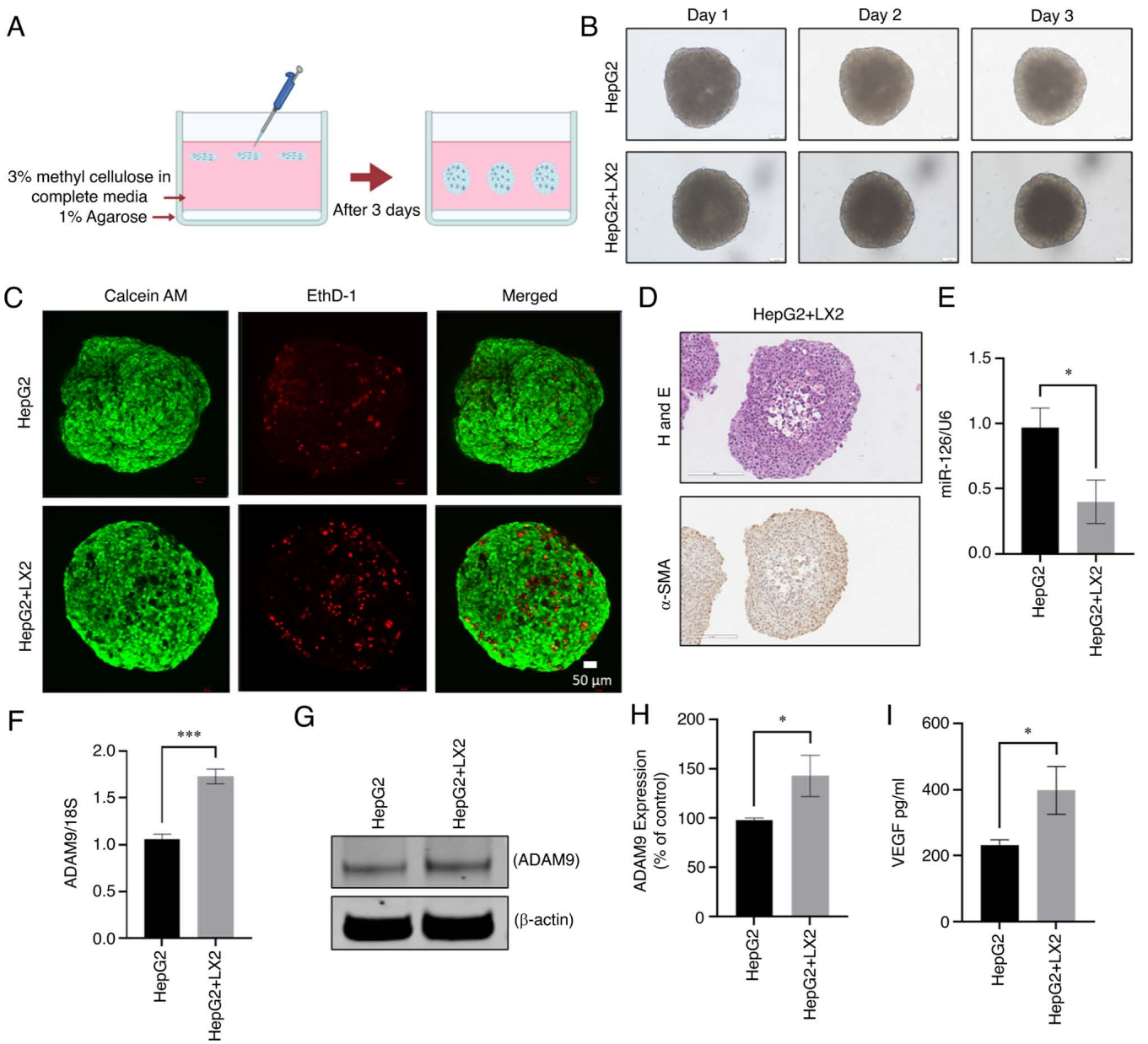

Figure 5. Generation and characterization of 3D co-culture spheroid model of HepG2 and LX2 cells. (A) Schematic presentation of 3D co-culture spheroid model by using methyl cellulose as a matrix. (B) Microscopic images of 3D MC of HepG2 and 3D CC of HepG2 and LX2 at days 1, 2 and 3 (scale bars, 50 μm). (C) Confocal imaging of 3D MC/CC spheroids with live/dead staining (green calcein AM staining indicated live cells, while red EtBr homodimer staining indicated dead cells; scale bars, 50 μm). (D) Microscopic images of hematoxylin and eosin staining of 3D CC spheroids represent cell arrangement and immunohistochemical staining for α-SMA (scale bars, 200 μm). (E) The expression of miR-126-3p in 3D MC and 3D CC spheroids was determined by Real time-qPCR. Data represent the fold change relative to the control after normalization to 18s rRNA as an internal control. (F and G) ADAM9 in 3D MC and CC was determined (F) by real time-qPCR at the RNA level and (G) western blot at the protein level. (H) Densitometric quantification of the relative expression of ADAM9 from the western blots normalized to β-actin. (I) The level of VEGF secretion from the 3D MC and CC spheroids was measured by ELISA. Values are expressed as the mean ± standard deviation (n=3 replicates). *P<0.05, ***P<0.001. ADAM9, disintegrin and metalloproteinase domain-containing protein 9; α-SMA, α-smooth muscle actin; CC, co-culture; MC, monoculture; EtBr, ethidium bromide; VEGF, vascular endothelial growth factor.

to regulate HSC viability and fibrinogenesis (36). Thus, elucidating the mechanisms of LC interactions is important in order to understand the contributions of the stromal cells or fibrotic milieu on tumor growth and progression.

Extracellular vesicles may serve as vehicles for mediators of intercellular crosstalk between the cells within the TME. To mimic the interaction between LC cells and their microenvironment, the potential contribution of EV non-coding RNA crosstalk between cell types was evaluated using *in vitro* cell co-culture models and cell spheroid models. Co-culture studies have been widely used to study inter-cellular crosstalk between LC cells and HSCs to understand the microenvironmental impact on cancer progression. To study cargo within EVs released from either cell, the cell supernatant and the EVs released within the supernatant were collected. In the present study, alterations in EV-RNA and phenotypic alterations in co-culture compared with monoculture conditions were identified. While an analysis of cellular effects and associated phenotypes related to vesicles released from cells in monoculture is certainly of interest,

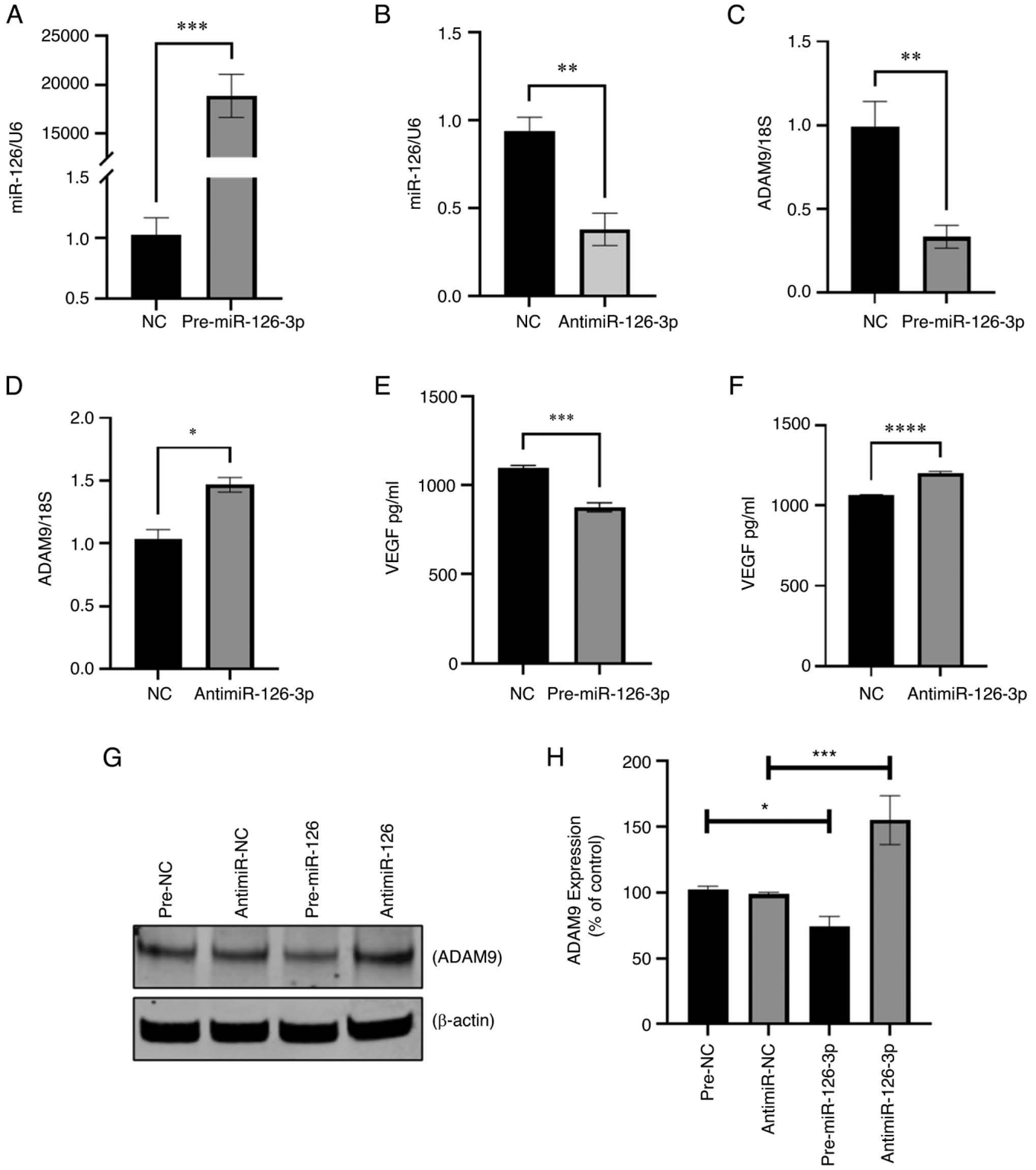

Figure 6. Effect of pre-miR-126-3p/antimiR-126-3p on 3D CC spheroids. Expression of miR-126 after transfection of (A) pre-miR-126-3p and (B) AntimiR-126-3p by Lipofectamine 3000 in 3-day-old CC spheroids of HepG2 and LX2 cells. (C and D) Expression of ADAM9 at the RNA level by real time-quantitative PCR after transfection of (C) pre-miR-126-3p or (D) antimiR-126-3p. (E and F) Measurement of VEGF secretion after manipulation of the level of miR-126 expression with (E) pre-miR-126-3p or (F) antimiR-126-3p. (G) Expression of ADAM9 at the protein level was determined by western blot. (H) Densitometric quantification of the relative expression of ADAM9; β-actin was used as the internal control for normalization of the western blot data. Values are expressed as the mean ± standard deviation (n=3 replicates). *P<0.05, **P<0.01, ***P<0.001, ****P<0.0001. ADAM9, disintegrin and metalloproteinase domain-containing protein 9; CC, co-culture; VEGF, vascular endothelial growth factor; miR, microRNA; NC, negative control.

and should be conducted, the systematic characterization and analysis of the associated phenotypes is beyond the scope of the present study.

Recent studies on EVs as a carrier of information between cells in the microenvironment have garnered much attention. Indirect co-culture of tumor-endothelial cells has indicated

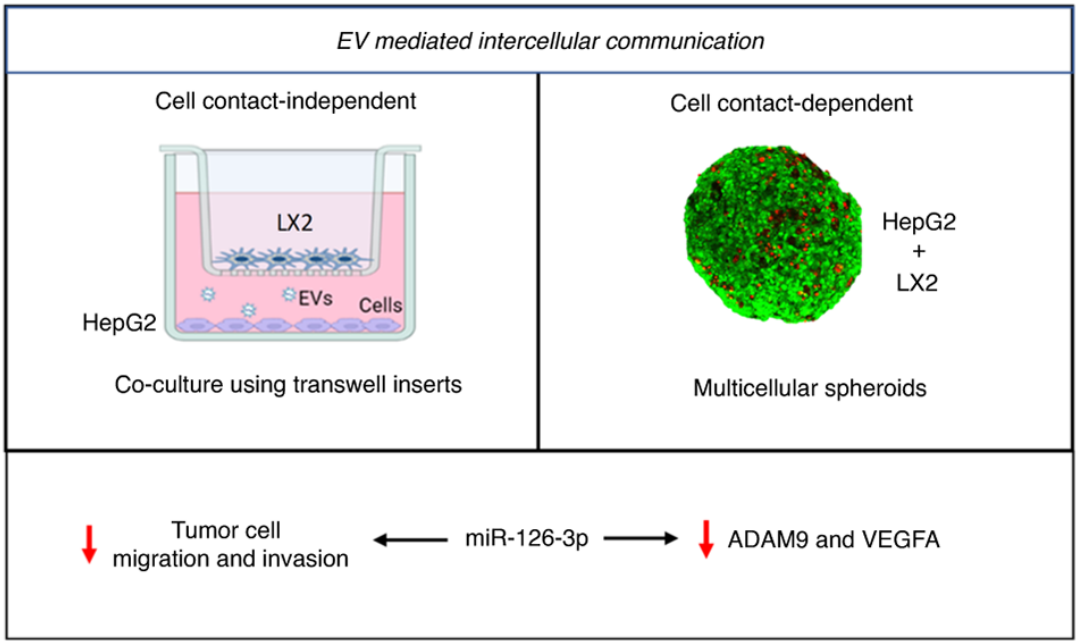

Figure 7. EV-mediated RNA communication in the LC TME. The image depicts intercellular EV-based cell contact-independent and -dependent communication in 2D and 3D co-culture models of the LC TME. The figure was generated using BioRender.com. EVs, extracellular vesicles; VEGF, vascular endothelial growth factor; miR, microRNA; LC, liver cancer; TME, tumor microenvironment.

that EVs laden with stimulating factors are released by tumor cells and may be taken up by endothelial cells, inducing proliferation and reduction of apoptosis (37). LC-derived EVs deliver 14-3-3ζ to tumor-infiltrating T lymphocytes (TILs), inhibiting their antitumor functions (38). EVs from macrophages exposed to apoptotic cancer cells have increased IL-6 that leads to phosphorylation of STAT3 and increased transcription of target genes inducing proliferation and migration in breast cancer cells (39).

In the present study, a systematic assessment of EV miRNA was performed using next-generation sequencing. Of note, changes in a select number of miRNAs were observed when HepG2 cells were co-cultured with LX-2 cells. Communication between tumor cells and stromal elements may have a key role in cancer progression. EV-mediated transfer of miRNAs, such as miR-122 (40), miR-21 and miR-192 (41), has been reported. The EV cargo comprises numerous diverse types of biomolecules, including small RNA, such as miRNAs, which may have other downstream effects in target cells following their transfer. EV-mediated transfer of miRNA has been implicated in numerous different settings (19), including Twist1 (42), k-ras (43) miR-122 (44) miR-200 (45). HSC EVs were reported to transfer miR-335-5p to inhibit proliferation and invasion in target LC cells (46), while LC-derived EV miR-21 was indicated to transform HSCs into cancer-associated fibroblasts (CAFs) to promote cancer progression (47). Similarly, miR-1247-3p in EVs from tumor cells was able to convert normal fibroblasts to CAFs (48).

An increase in miR-126-3p in EVs occurs when LC cells are co-cultured with HSCs. Of note, miR-126-3p has been indicated to have a tumor-suppressive role in LC and other cancers. Indeed, low intratumoral expression of miR-126-3p is associated with recurrence and poor survival of patients with HCC, whereas forced overexpression markedly impairs HCC tumor cell proliferation, invasion and development of metastatic lung nodules (49,50). Therefore, the present study aimed to further explore the role of miR-126-3p in the liver TME. While modulation of miR-126-3p altered migration and invasion of human LC cells in the present study, there was no appreciable difference in sensitivity to drugs, in the proliferative capacity in 2D cultures or in size or number of tumor-cell spheroids in 3D culture. However, other studies reported that miR-126-3p is able to inhibit not only the migration and invasion, but also the proliferation of tumor cells and tumor angiogenesis *in vitro* and *in vivo* in HCC tumor-bearing mice (50,51). These effects are mediated by modulation of downstream targets such as low-density lipoprotein related protein 6 (50) and ADAM9 (52) to suppress tumor metastasis, phosphoinositide-3-kinase regulatory subunit 2 to impair tumor cell migration/invasion and epidermal growth factor like domain 7 to inhibit tumor angiogenesis (50). Validation of miR-126-mediated regulation of ADAM9 expression has been extensively reported, including an *in vitro* 3'UTR luciferase assay (53) and by target seed sequence prediction software (52,54); therefore, it was not further validated in the present study. The role of miR-126 in modulating sensitivity to therapy has been noted with altered sensitivity to cisplatin in HCC through the repression of insulin receptor substrate 1 expression (55), or to sorafenib through the downregulation of sprout-related EVH1 domain-containing protein 1 (56). MiR-126-3p has also been indicated to elicit tumor suppressor effects in other gastrointestinal and other solid tumor types, such as lung cancer (57,58).

Manipulation of extracellular RNA signaling may have therapeutic implications. A single miRNA may regulate the expression of multiple genes, thus making them worthwhile targets for therapeutic approaches (59,60). Specific miRNAs, such as miR-126-3p, have a growing body of evidence for multiple tumor-suppressive roles that may be mediated

through multiple targets. While diverse EV-RNAs may be present in the local TME and may theoretically participate in EV-RNA signaling across cells, studies focused on a single candidate HSC-derived EV-RNA demonstrate the functional contribution of EV-RNA signaling across cells in the local microenvironment to modulate LC cell behavior. With this observation, determining the contributions of other candidates or their combinatorial effects on local microenvironmental cell-to-cell signaling is justified. These studies enable us to understand the contributions of EV-based miR-126-3p-mediated intercellular communication on tumor behavior. Based on these findings, enrichment of miR-126-3p in LC cells may be used as a therapeutic approach to inhibit tumor growth through manipulated expression of key mediators, such as ADAM9 and VEGFA, to modulate critical processes involved in tumor growth, such as metastasis or angiogenesis (Fig. 7). However, further studies should be performed to explore other downstream targets of miR-126-3p in the liver TME.

Acknowledgements

The authors would like to acknowledge Dr. Gregory j Gores (Division of Gastroenterology and Hepatology, Mayo Clinic, Rochester, Minnesota, USA) for providing the LX2 cell line.

Funding

The present study was supported by the National Cancer Institute (grant no. CA217833), the James C. and Sarah K. Kennedy Deanship and the Alfred D. and Audrey M. Petersen Professorship to TP.

Availability of data and materials

The dataset for RNA-sequencing presented in this study may be obtained from the online repository Gene Expression Omnibus (GEO) under accession no. GSE196131 (https://www.ncbi.nlm.nih.gov/geo/query/acc.cgi?acc=GSE196131). The data may be accessed using the password 'mxsnqoawhnchnet' on the above link. The datasets used and/or analyzed during the current study are available from the corresponding author upon reasonable request.

Authors' contributions

Conceptualization, TP; methodology, TP, AM, PG, AAS and JD; formal analysis, AM, PG and AAS; investigation, AM, PG, AAS, JD, IY and TP; resources, TP; data curation, AM, PG and AAS; writing-original draft, TP, AM and PG; writing-review & editing, AM, PG, AAS, IY, TP and JD; visualization, AM and PG; supervision, TP; funding acquisition, TP. The authenticity of the raw data has been verified by AM, PG, AAS and TP. All authors have read and approved the final version of the manuscript.

Ethics approval and consent to participate

Not applicable.

Patient consent for publication

Not applicable.

Competing interest

The authors declare that they have no competing interests.

References

1. Mbeunkui F and Johann DJ Jr: Cancer and the tumor microenvironment: A review of an essential relationship. Cancer Chemother Pharmacol 63: 571-582, 2009.
2. Hanahan D and Weinberg RA: Hallmarks of cancer: The next generation. Cell 144: 646-674, 2011.
3. Wang X, Hassan W, Jabeen Q, Khan GJ and Iqbal F: Interdependent and independent multidimensional role of tumor microenvironment on hepatocellular carcinoma. Cytokine 103: 150-159, 2018.
4. Tahmasebi Birgani M and Carloni V: Tumor microenvironment, a paradigm in hepatocellular carcinoma progression and therapy. Int J Mol Sci 18: 405, 2017.
5. Kamil F and Rowe JH: How does the tumor microenvironment play a role in hepatobiliary tumors? J Gastrointest Oncol 9: 180-195, 2018.
6. Balogh J, Victor D III, Asham EH, Burroughs SG, Boktour M, Saharia A, Li X, Ghobrial RM and Monsour HP Jr: Hepatocellular carcinoma: A review. J Hepatocell Carcinoma 3: 41-53, 2016.
7. Yang S, Yang L, Li X, Li B, Li Y, Zhang X, Ma Y, Peng X, Jin H and Li H: New insights into autophagy in hepatocellular carcinoma: Mechanisms and therapeutic strategies. Am J Cancer Res 9: 1329-1353, 2019.
8. Baglieri J, Brenner DA and Kisseleva T: The role of fibrosis and liver-associated fibroblasts in the pathogenesis of hepatocellular carcinoma. Int J Mol Sci 20: 1723, 2019.
9. Song Y, Kim SH, Kim KM, Choi EK, Kim J and Seo HR: Activated hepatic stellate cells play pivotal roles in hepatocellular carcinoma cell chemoresistance and migration in multicellular tumor spheroids. Sci Rep 6: 36750, 2016.
10. Laurenzana I, Lamorte D, Trino S, De Luca L, Ambrosino C, Zoppoli P, Ruggieri V, Del Vecchio L, Musto P, Caivano A and Falco G: Extracellular vesicles: A new prospective in crosstalk between microenvironment and stem cells in hematological malignancies. Stem Cells Int 2018: 9863194, 2018.
11. Bebelman MP, Smit MJ, Pegtel DM and Baglio SR: Biogenesis and function of extracellular vesicles in cancer. Pharmacol Ther 188: 1-11, 2018.
12. Jabalee J, Towle R and Garnis C: The role of extracellular vesicles in cancer: Cargo, function, and therapeutic implications. Cells 7: 93, 2018.
13. Yang J, Li C, Zhang L and Wang X: Extracellular vesicles as carriers of non-coding RNAs in liver diseases. Front Pharmacol 9: 415, 2018.
14. Vu LT, Peng B, Zhang DX, Ma V, Mathey-Andrews CA, Lam CK, Kiomourtzis T, Jin J, McReynolds L, Huang L, *et al*: Tumor-secreted extracellular vesicles promote the activation of cancer-associated fibroblasts via the transfer of microRNA-125b. J Extracell Vesicles 8: 1599680, 2019.
15. Au Yeung CL, Co NN, Tsuruga T, Yeung TL, Kwan SY, Leung CS, Li Y, Lu ES, Kwan K, Wong KK, *et al*: Exosomal transfer of stroma-derived miR21 confers paclitaxel resistance in ovarian cancer cells through targeting APAF1. Nat Commun 7: 11150, 2016.
16. Lee H, Abston E, Zhang D, Rai A and Jin Y: Extracellular vesicle: An emerging mediator of intercellular crosstalk in lung inflammation and injury. Front Immunol 9: 924, 2018.
17. Xu L, Hui A, Albanis E, Arthur MJ, O'Byrne SM, Blaner WS, Mukherjee P, Friedman SL and Eng FJ: Human hepatic stellate cell lines, LX-1 and LX-2: New tools for analysis of hepatic fibrosis. Gut 54: 142-151, 2005.
18. Sayyed AA, Gondaliya P, Mali M, Pawar A, Bhat P, Khairnar A, Arya N and Kalia K: MiR-155 inhibitor-laden exosomes reverse resistance to cisplatin in a 3D tumor spheroid and xenograft model of oral cancer. Mol Pharm 18: 3010-3025, 2021.

19. Matsuda A, Ishiguro K, Yan IK and Patel T: Extracellular vesicle-based therapeutic targeting of β-catenin to modulate anticancer immune responses in hepatocellular cancer. Hepatol Commun 3: 525-541, 2019.
20. Kogure T and Patel T: Isolation of extracellular nanovesicle microRNA from liver cancer cells in culture. In: Kosaka N (eds) Circulating MicroRNAs. Methods in Molecular Biology. Vol. 1024. Humana Press, Totowa, NJ, pp11-18, 2013.
21. Schmittgen TD and Livak KJ: Analyzing real-time PCR data by the comparative C(T) method. Nat Protoc 3: 1101-1108, 2008.
22. Sharma N, Soni R, Sharma M, Chatterjee S, Parihar N, Mukarram M, Kale R, Sayyed AA, Behera SK and Khairnar A: Chlorogenic acid: A polyphenol from coffee rendered neuroprotection against rotenone-induced parkinson's disease by GLP-1 secretion. Mol Neurobiol 59: 6834-6856, 2022.
23. Parekh P, Sharma N, Sharma M, Gadepalli A, Sayyed AA, Chatterjee S, Kate A and Khairnar A: AMPK-dependent autophagy activation and alpha-Synuclein clearance: A putative mechanism behind alpha-mangostin's neuroprotection in a rotenone-induced mouse model of Parkinson's disease. Metab Brain Dis: Sep 30, 2022 (Epub ahead of print).
24. Gondaliya P, Sayyed AA, Bhat P, Mali M, Arya N, Khairnar A and Kalia K: Mesenchymal stem cell-derived exosomes loaded with miR-155 inhibitor ameliorate diabetic wound healing. Mol Pharm 19: 1294-1308, 2022.
25. Takahashi K, Yan IK, Kogure T, Haga H and Patel T: Extracellular vesicle-mediated transfer of long non-coding RNA ROR modulates chemosensitivity in human hepatocellular cancer. FEBS Open Bio 4: 458-467, 2014.
26. Hsieh MH, Tsai JP, Yang SF, Chiou HL, Lin CL, Hsieh YH and Chang HR: Fisetin suppresses the proliferation and metastasis of renal cell carcinoma through upregulation of MEK/ERK-targeting CTSS and ADAM9. Cells 8: 948, 2019.
27. Kumar S, Davra V, Obr AE, Geng K, Wood TL, De Lorenzo MS and Birge RB: Crk adaptor protein promotes PD-L1 expression, EMT and immune evasion in a murine model of triple-negative breast cancer. Oncoimmunology 7: e1376155, 2017.
28. Guo C, Zhao D, Zhang Q, Liu S and Sun MZ: miR-429 suppresses tumor migration and invasion by targeting CRKL in hepatocellular carcinoma via inhibiting Raf/MEK/ERK pathway and epithelial-mesenchymal transition. Sci Rep 8: 2375, 2018.
29. Carpino G, Morini S, Ginanni Corradini S, Franchitto A, Merli M, Siciliano M, Gentili F, Onetti Muda A, Berloco P, Rossi M, *et al*: Alpha-SMA expression in hepatic stellate cells and quantitative analysis of hepatic fibrosis in cirrhosis and in recurrent chronic hepatitis after liver transplantation. Dig Liver Dis 37: 349-356, 2005.
30. Alhasan L: MiR-126 modulates angiogenesis in breast cancer by targeting VEGF-A-mRNA. Asian Pac J Cancer Prev 20: 193-197, 2019.
31. Amann T, Bataille F, Spruss T, Mühlbauer M, Gäbele E, Schölmerich J, Kiefer P, Bosserhoff AK and Hellerbrand C: Activated hepatic stellate cells promote tumorigenicity of hepatocellular carcinoma. Cancer Sci 100: 646-653, 2009.
32. Han S, Han L, Yao Y, Sun H, Zan X and Liu Q: Activated hepatic stellate cells promote hepatocellular carcinoma cell migration and invasion via the activation of FAK-MMP9 signaling. Oncol Rep 31: 641-648, 2014.
33. Yu G, Jing Y, Kou X, Ye F, Gao L, Fan Q, Yang Y, Zhao Q, Li R, Wu M and Wei L: Hepatic stellate cells secreted hepatocyte growth factor contributes to the chemoresistance of hepatocellular carcinoma. PLoS One 8: e73312, 2013.
34. Santamato A, Fransvea E, Dituri F, Caligiuri A, Quaranta M, Niimi T, Pinzani M, Antonaci S and Giannelli G: Hepatic stellate cells stimulate HCC cell migration via laminin-5 production. Clin Sci (Lond) 121: 159-168, 2011.
35. Ma T, Wang Z, Yang Z and Chen J: Cluster of differentiation 147 is a key molecule during hepatocellular carcinoma cell-hepatic stellate cell cross-talk in the rat liver. Mol Med Rep 12: 111-118, 2015.
36. Magistri P, Leonard SY, Tang CM, Chan JC, Lee TE and Sicklick JK: The glypican 3 hepatocellular carcinoma marker regulates human hepatic stellate cells via Hedgehog signaling. J Surg Res 187: 377-385, 2014.
37. Jamshidi-Parsian A, Griffin RJ, Kore RA, Todorova VK and Makhoul I: Tumor-endothelial cell interaction in an experimental model of human hepatocellular carcinoma. Exp Cell Res 372: 16-24, 2018.
38. Wang X, Shen H, Zhangyuan G, Huang R, Zhang W, He Q, Jin K, Zhuo H, Zhang Z, Wang J, *et al*: 14-3-3ζ delivered by hepatocellular carcinoma-derived exosomes impaired anti-tumor function of tumor-infiltrating T lymphocytes. Cell Death Dis 9: 159, 2018.
39. Yu X, Zhang Q, Zhang X, Han Q, Li H, Mao Y, Wang X, Guo H, Irwin DM, Niu G and Tan H: Exosomes from macrophages exposed to apoptotic breast cancer cells promote breast cancer proliferation and metastasis. J Cancer 10: 2892-2906, 2019.
40. Basu S and Bhattacharyya SN: Insulin-like growth factor-1 prevents miR-122 production in neighbouring cells to curtail its intercellular transfer to ensure proliferation of human hepatoma cells. Nucleic Acids Res 42: 7170-7185, 2014.
41. Chiba M, Kimura M and Asari S: Exosomes secreted from human colorectal cancer cell lines contain mRNAs, microRNAs and natural antisense RNAs, that can transfer into the human hepatoma HepG2 and lung cancer A549 cell lines. Oncol Rep 28: 1551-1558, 2012.
42. Sun T, Zhao N, Zhao XL, Gu Q, Zhang SW, Che N, Wang XH, Du J, Liu YX and Sun BC: Expression and functional significance of Twist1 in hepatocellular carcinoma: Its role in vasculogenic mimicry. Hepatology 51: 545-556, 2010.
43. Tao J, Zhang R, Singh S, Poddar M, Xu E, Oertel M, Chen X, Ganesh S, Abrams M and Monga SP: Targeting β-catenin in hepatocellular cancers induced by coexpression of mutant β-catenin and K-Ras in mice. Hepatology 65: 1581-1599, 2017.
44. Hsu SH, Wang B, Kota J, Yu J, Costinean S, Kutay H, Yu L, Bai S, La Perle K, Chivukula RR, *et al*: Essential metabolic, anti-inflammatory, and anti-tumorigenic functions of miR-122 in liver. J Clin Invest 122: 2871-2883, 2012.
45. Xue X, Zhang Y, Zhi Q, Tu M, Xu Y, Sun J, Wei J, Lu Z, Miao Y and Gao W: MiR200-upregulated Vasohibin 2 promotes the malignant transformation of tumors by inducing epithelial-mesenchymal transition in hepatocellular carcinoma. Cell Commun Signal 12: 62, 2014.
46. Wang F, Li L, Piontek K, Sakaguchi M and Selaru FM: Exosome miR-335 as a novel therapeutic strategy in hepatocellular carcinoma. Hepatology 67: 940-954, 2018.
47. Zhou Y, Ren H, Dai B, Li J, Shang L, Huang J and Shi X: Hepatocellular carcinoma-derived exosomal miRNA-21 contributes to tumor progression by converting hepatocyte stellate cells to cancer-associated fibroblasts. J Exp Clin Cancer Res 37: 324, 2018.
48. Fang T, Lv H, Lv G, Li T, Wang C, Han Q, Yu L, Su B, Guo L, Huang S, *et al*: Tumor-derived exosomal miR-1247-3p induces cancer-associated fibroblast activation to foster lung metastasis of liver cancer. Nat Commun 9: 191, 2018.
49. Chen H, Miao R, Fan J, Han Z, Wu J, Qiu G, Tang H and Peng Z: Decreased expression of miR-126 correlates with metastatic recurrence of hepatocellular carcinoma. Clin Exp Metastasis 30: 651-658, 2013.
50. Du C, Lv Z, Cao L, Ding C, Gyabaah OA, Xie H, Zhou L, Wu J and Zheng S: MiR-126-3p suppresses tumor metastasis and angiogenesis of hepatocellular carcinoma by targeting LRP6 and PIK3R2. J Transl Med 12: 259, 2014.
51. Gong C, Fang J, Li G, Liu HH and Liu ZS: Effects of microRNA-126 on cell proliferation, apoptosis and tumor angiogenesis via the down-regulating ERK signaling pathway by targeting EGFL7 in hepatocellular carcinoma. Oncotarget 8: 52527-52542, 2017.
52. Xiang LY, Ou HH, Liu XC, Chen ZJ, Li XH, Huang Y and Yang DH: Loss of tumor suppressor miR-126 contributes to the development of hepatitis B virus-related hepatocellular carcinoma metastasis through the upregulation of ADAM9. Tumour Biol 39: 1010428317709128, 2017.
53. Hamada S, Satoh K, Fujibuchi W, Hirota M, Kanno A, Unno J, Masamune A, Kikuta K, Kume K and Shimosegawa T: MiR-126 acts as a tumor suppressor in pancreatic cancer cells via the regulation of ADAM9miR-126/ADAM9 regulates invasive growth of pancreatic cancer. Mol Cancer Res 10: 3-10, 2012.
54. Jia AY, Castillo-Martin M, Bonal DM, Sánchez-Carbayo M, Silva JM and Cordon-Cardo C: MicroRNA-126 inhibits invasion in bladder cancer via regulation of ADAM9. Br J Cancer 110: 2945-2954, 2014.
55. Zuo J, Luo R, Huang C, Lou X and Li L: MiR-126 enhances cisplatin chemosensitivity in hepatocellular carcinoma cells by targeting IRS1. Trop J Pharm Res 18: 25-30, 2019.
56. Tan W, Lin Z, Chen X, Li W, Zhu S, Wei Y, Huo L, Chen Y and Shang C: miR-126-3p contributes to sorafenib resistance in hepatocellular carcinoma via downregulating SPRED1. Ann Transl Med 9: 38, 2021.

57. Hu M, Xiong S, Chen Q, Zhu S and Zhou X: Novel role of microRNA-126 in digestive system cancers: From bench to bedside. Oncol Lett 17: 31-41, 2019.
58. Miko E, Margitai Z, Czimmerer Z, Várkonyi I, Dezso B, Lányi A, Bacsó Z and Scholtz B: miR-126 inhibits proliferation of small cell lung cancer cells by targeting SLC7A5. FEBS Lett 585: 1191-1196, 2011.
59. Kitano M and Bloomston PM: Hepatic stellate cells and microRNAs in pathogenesis of liver fibrosis. J Clin Med 5: 38, 2016.
60. Sayyed AA, Gondaliya P, Bhat P, Mali M, Arya N, Khairnar A and Kalia K: Role of miRNAs in cancer diagnostics and therapy: A recent update. Curr Pharm Des 28: 471-487, 2022.